Renewable Energy 233 (2024) 121078

Contents lists available at ScienceDirect

Renewable Energy

journal homepage: www.elsevier.com/locate/renene

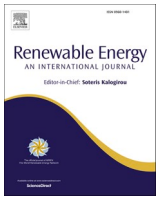

Characterization of solar-derivate ultraviolet radiation for water solar treatment applications

Lisdelys González-Rodríguez [a,b], Alejandro Cabrera-Reina [c], Jorge Rosas [d], Matías Volke [e], Aitor Marzo [f,*]

[a] Facultad de Ingeniería y Negocios, Universidad de Las Américas, Sede Concepción, Chile
[b] Núcleo de Investigación en Data Science (NIDS), Facultad de Ingeniería y Negocios, Universidad de Las Américas, Santiago, Chile
[c] Universidad Tecnológica Metropolitana, Santiago de Chile, Chile
[d] Instituto de Ciencias Atmosféricas, Universidad de Sao Paulo, Sao Paulo, Brazil
[e] Facultad de Ingeniería, Universidad de Concepción, Concepción, Chile
[f] Departamento de Óptica, Universidad de Granada, Granada, Spain

ARTICLE INFO

Keywords:
Solar ultraviolet radiation
Solar spectral irradiance
LibRadtran
MODIS
Water solar treatment
Solar energy

ABSTRACT

Water resources are under increasing pressure from ever-increasing demand from industry and society. However, water is a limited resource that must be sustainable and protected. This problem is highlighted in desert areas, where water quality and abundance are scarce. Solar-powered water treatment systems are an inexpensive solution to ensure water quality for human consumption. This research analyzes solar ultraviolet radiation (UVR) in three populated Chilean cities to study the potential feasibility of the solar-powered photo-Fenton process for wastewater remediation. To generate long-term UVR values, satellite and reanalysis data and the Radiative Transfer Model were used. Results show high daily levels of solar ultraviolet irradiation, 1299.95kJm^{-2} for Antofagasta. The shortest treatment time for summer operation was observed in Santiago (21 min), followed by Antofagasta (34 min), and Concepción (35 min). Santiago presented the lowest volume of photoreactors during the summer (297 L) and Antofagasta during the winter (1589 L). This is the first preliminary analysis showing the possibilities of exploiting the potential of UVR in Chilean cities to provide tools for integrating water treatment technologies. This research motivates further studies on spectral radiation and emerging advanced oxidation technologies and the development of prospects for water and wastewater treatment.

1. Introduction

Solar ultraviolet radiation (UVR) data at the Earth's surface are essential for studying and designing water treatment systems that use solar energy. The UVR region covers the wavelength range of 100–400 nm and is divided into three bands: UVR-C (100–280 nm), UVR-B (280–315 nm), and UVR-A (315–400 nm) (Madronich Sasha, 1993). In terms of irradiance (Wm^{-2}), the amount of UVR arriving at the surface is lower than in the visible (VIS) and infrared (IR) ranges. However, the intrinsic energy of the photon is inversely proportional to its wavelength, so photons in the ultraviolet are more energetic. The high energy of UVR photons allows them to break chemical bonds, making them a type of ionizing radiation. This property makes UVR harmful to living organisms [1,2] and materials that are exposed to it, which has a significant role in many solar applications. For instance, in solar water treatment systems, UVR is often used to initiate photocatalytic reactions that degrade several water pollutants [3–5]. Therefore, knowing the UVR incident on the Earth's surface is relevant given the spectral selectivity of UVR on many photocatalytic solar systems.

The influences of UVR on many photocatalytic solar systems have been studied [3,4,6] mainly, using TiO_2 as a semiconductor material [7,8] or iron salts in the case of the homogeneous photocatalytic process named photo-Fenton [3,9,10]. The principles of these processes are mainly based on the generation of strongly oxidizing radicals, such as hydroxyl radical ($^{\bullet}OH$), that result in the non-selective oxidation of diverse organic compounds. The radicals are generated on the surface of the wideband-gap semiconductor upon excitation (usually) with $<$400 nm UVR and the formation of an electron-hole pair in the TiO_2 material, while in the photo-Fenton process, these are generated thanks to the reaction between iron salts and hydrogen peroxide. The ability of UVR

* Corresponding author.
E-mail address: aitorm@ugr.es (A. Marzo).

https://doi.org/10.1016/j.renene.2024.121078
Received 9 January 2024; Received in revised form 22 July 2024; Accepted 25 July 2024
Available online 14 August 2024

to photodegrade, under catalytic conditions, a wide range of pollutants has been extensively demonstrated in the literature, serving as an example of Bisphenol A [11], Oxamyl [3], Oxytetracycline [12], and Spiramycin [8]. Generally, the degradation of pollutants increases with increasing UVR, from 20 to 30 Wm^{-2} (0.2–0.3 mol photons $m^{-2}h^{-1}$ in the 300–400 nm) [4], showing a linear dependence. Above 30 Wm^{-2}, several authors have found that process efficiency reaches a plateau [13], although this obviously will depend on different issues such as the photoreactor, catalyst characteristics, concentration, type of wastewater, etc. In any case and up to a certain limit, high UVR values may enhance photocatalytic performance.

In the water/wastewater treatment process, solar energy represents a sustainable, safe, and abundant resource and its use avoids potential contamination associated with lamps (mercury, electric consumption, etc.) [14]. Therefore, the integration of solar energy in the photocatalytic processes is an active strategy aligned with the current international concept of sustainability. UVR data is a prerequisite for the development of solar water treatments because this information in combination with temperature is essential in predicting solar water treatment efficacy [15]. In general, it has been reported that increasing the operating temperature always has a beneficial effect on the reaction kinetics of the photo-Fenton process [4]. However, for temperatures above 50 °C, iron precipitation has been observed [16]. In any case, within normal ambient temperature ranges, higher temperatures always lead to a higher efficiency of the decontamination process [17]. found that the site location and ambient conditions (temperature, UVR levels, and availability of sufficient sunlight) are determinants in the solar photo-Fenton treatment efficiency. Dynamic models coupled to instant solar UVR and water temperature data can be used to know when the process has reached the treatment goal [18,19] or even can be useful to develop optimized reagents dosage schemes [20]. When overcast conditions are frequent, the availability of sufficient sunlight is scarce, and therefore the photocatalytic process requires more time for water treatment [11]. However [21], using the solar photo-Fenton process found that 70 % of organic contaminants can be removed both in winter and summer in competitive times. Considering the water pollution issues in Chile [22–26], solar photocatalysis presents itself as a promising technology for water treatment. The solar photo-Fenton process uses a renewable and pollution-free energy source, sunlight, which is abundant, particularly in certain regions such as northern Chile, receiving over 4000 h of sunlight annually [17]. Chile's lack of comprehensive data regarding the distribution of UVR resources underscores the imperative to uncover this information. The main sources for obtaining UVR datasets include empirical models [27], radiative transfer model (RTM) [28], remote sensing [29], and ground-based measurement [30]. Ground-based measurements using spectroradiometers provide accurate data for local spectral radiation intensity. However, the high cost of these devices, coupled with the necessity for high operating and maintenance costs limit their measurements to a few locations and/or limited measurement campaigns [31]. Alternatively, by combining RTM, satellite, and reanalysis datasets long-term UVR data can be produced. Among the available satellite and reanalysis data that provide atmospheric products with acceptable accuracy and high spatiotemporal continuity are Moderate Resolution Imaging Spectroradiometer (MODIS) [32], Modern-Era Retrospective Analysis for Research and Applications (MERRA2) [33], and European Centre for Medium-Range Weather Forecasts Reanalysis v5 (ERA5) [34]. In Ref. [34] developed a physical model for estimating surface solar UVR broadband in clear sky conditions from MERRA2 reanalysis products with high accuracy and strong robustness. Besides [35], presented a method to retrieve UVR data based on Lookup-tables (LUTs) and satellite-derived historical data at Ispra, Italy (45.81°N, 8.63°E) showing excellent results. Other authors [36,37] have suggested that applying similar methods to retrieve UVR is fast and has good accuracy. An RTM is a numerical solution of the radiative transfer equation, which includes all the radiative processes between the atmosphere and radiation, such as the scattering and absorption in the shortwave spectrum [38]. This model allows us to use as input detailed information on aerosols, total ozone column, total water vapor, surface albedo, clouds, distance earth-sun, latitude, solar zenith angle (SZA), and altitude. Therefore, it is possible to use it with long-term atmospheric databases for UVR estimations on a regional or national scale since they require a detailed description of the site and the thermodynamic state of the atmosphere.

Some radiative transfer codes are Tropospheric Ultraviolet–Visible radiative transfer (TUV); Simple Model of the Atmospheric Radiative Transfer of Sunshine (SMARTS2) [39]; MODerate resolution TRANsmission model (MODTRAN) [40], and Library for Radiative Transfer (LibRadtran) [28,38,41,42] Among them, LibRadtran has been recognized as a powerful tool, where simulations showed good accuracy in derived UVR [28,42]. The core program of LibRadtran is the freely radiative transfer tool UVSPEC which calculates the radiative field in the Earth's atmosphere [38].

In Chile, few reports have used RTM to derivate long-term UVR values. In the south of Chile (at 39°S) [43], used the DISORT code (Discrete Ordinate) and analyzed the ultraviolet erythemal doses. More recently [39], used the SMARTS code, demonstrating the importance of knowing the local solar spectrum characteristics in areas of photovoltaic and Concentrated Solar Power systems development. Meanwhile, [28]; and [44] used LibRadtran to develop UVR climatological maps for the Atacama Desert. The collaboration between the Chilean Ministry of Energy and USCAH-FCFM-Universidad de Chile [40] based on MODTRAN offers spectral predictions for the north macrozone. However, although the research provides reliable estimates of surface UVR, they focused on northern Chile leaving out the most populated areas of south-central Chile. Similarly, the assessment of UVR levels and their correlation with solar photo-Fenton process efficiency, essential for evaluating the feasibility of solar water treatment across Chile, represents a significant knowledge gap demanding attention. So, the goal of this research is to obtain reliable long-term UVR values from RTM simulation, satellite, and reanalysis data for populated Chilean cities located between 23°S and 37°S; to characterize solar-derivate ultraviolet radiation values and preliminary evaluate the feasibility of employing solar photo-Fenton process for water treatment in these populated cities.

2. Materials and methods

2.1. Study area

Fig. 1a and b shows the geographic position of Chile in South America, located between 17° 30′ and 56° 30′ South latitude and occupies a long coastal strip between the Andes mountains and the Pacific Ocean in the southwestern part of South America. It has an area of 756,102 km^2, where the capital and largest city is Santiago de Chile with more than 7 million inhabitants [45]. Chile is a very privileged country due to its solar energy potential, especially in the Northern regions that present one of the highest levels of radiation on the planet. Chile receives between 900 and 2200 $kWhm^{-2}$ of energy per year from the sun [46] Three Chilean cities between the latitude of −23°S and −37°S were selected for this study. The selection includes the largest number of inhabitants in the country, great economic, and industrial activity, and excellent areas for solar utilization based on [47]. According to the Köppen climate classification, Concepcion and Santiago have a warm-summer Mediterranean climate (Csb) (Fig. 1e and f). In contrast, in Antofagasta the cold semi-arid climate (BWk) climate predominates (Fig. 1d). Table 1 shows the main features of the study location.

2.2. Satellite and reanalysis data

The cloud fraction (CF, %). Total column ozone (O_3, DU) and total water vapor (WV, mm) were obtained from ERA5 for more than 30 years from 1979 to 2019. These data are available on the ERA5 website (htt

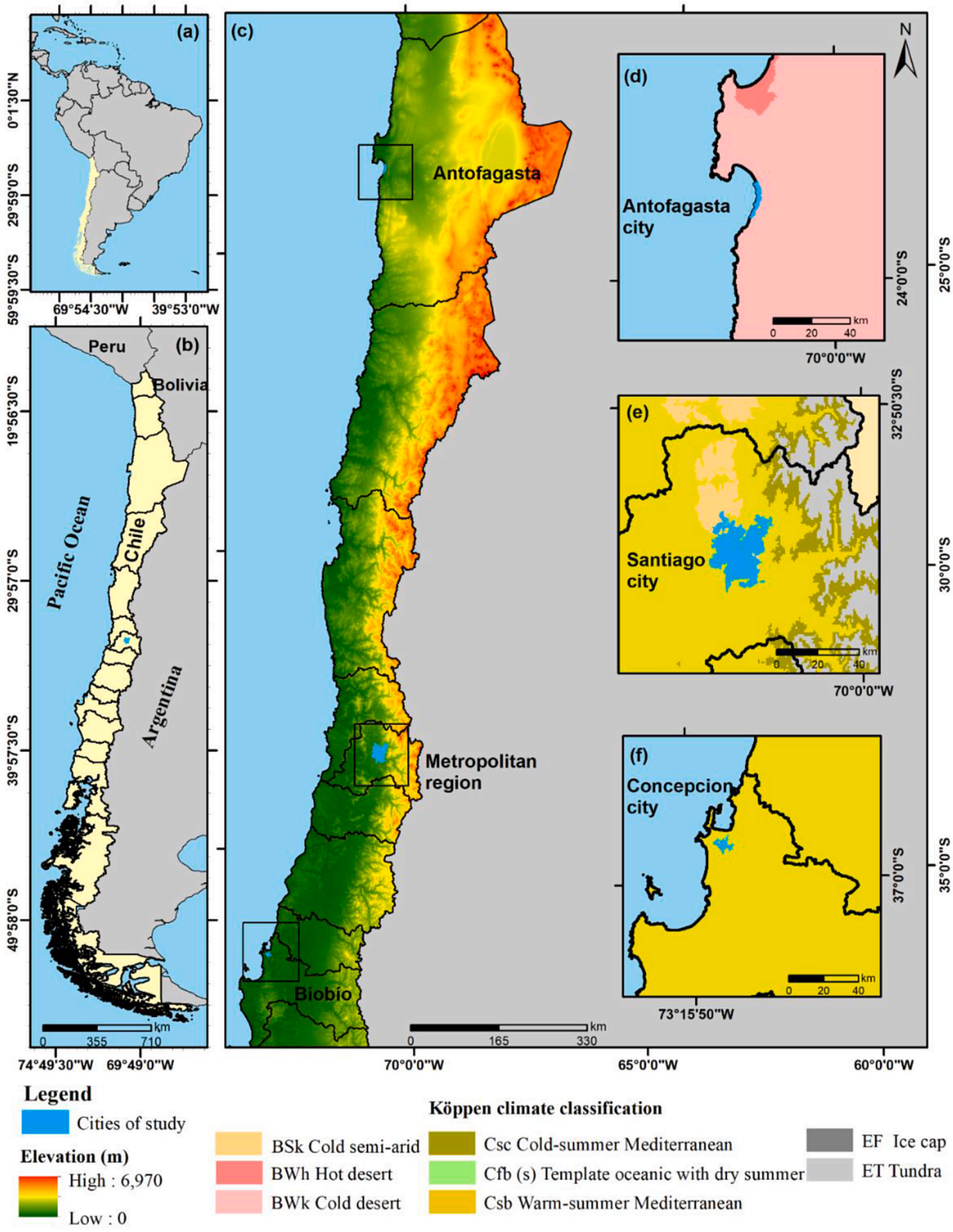

Fig. 1. (a) Geographic position of Chile in South-American (b) regional division in Chile, (c) topography present from the Antofagasta to Bio region, and (d–g) climate following Köppen classification. The elevation, distribution, and Köppen classification of regions were created using an ArcGIS analysis of a shapefile. The shapefiles and profile elevation were obtained from IDE.

ps://www.ecmwf.int/) with a 25 km resolution [48]. Aerosol optical depth (AOD, nm) or atmospheric turbidity is the product of particle density and the probability of interception of radiation, usually between 0.09 and 1 [50]. The aerosol values at 550 nm (AOD550) were found in Modern-Era Retrospective analysis for Research and Applications (MERRA, https://gmao.gsfc.nasa.gov/) with a spatial resolution of approx. 50 km [33]. Gueymard and Yang (2020) evaluated the AOD550 of MERRA2. This was achieved by comparing it with values obtained at AERONET ground-based stations around the World. For South America, the reported RMSE was 0.113 for an average AOD of 0.152, which

Table 1
Features of the study location.

Cities	Latitude (°S)	Longitude (°W)	Altitude (m.a.s.l)	Climate (Köppen)	Region	Inhabitants[a] (hab)
Antofagasta	−23.59	−70.39	150	BWk	Antofagasta	607,534
Santiago	−33.49	−70.73	500	Csb	Metropolitan	7112.808
Concepcion	−36.73	−72.46	121	Csb	Biobío	2037.414

[a] Hab Census 2017.

represents a 74 % error in relative terms. The outcome is not contingent on geographical location. Consequently, it is essential to consider local conditions. In a previous study, Agustín Laguarda & Gonzalo Abal [49] compared MERRA2 AOD550 with three AERONET sites in Argentina and Brazil, which had similar latitudes to those used in the present study. They reported an RMSE of approximately 33 % for AOD550. While some authors have indicated that elevated uncertainty values in the AOD do not inherently result in an augmented error in the estimation of broadband atmospheric radiative transfer or broadband cumulative irradiance [50,51], it is imperative to exercise caution in considering the potential impact of this uncertainty on the ultraviolet band. Considering the aforementioned considerations, it is imperative to corroborate the data with ground measurements. The methodology employed in this process is elucidated in the subsequent section.

Finally, the Global solar irradiance (IG, 0.3μm–4μm), will be obtained from MODIS (MCD18A1 product) with 3 h at time resolution (9:00, 12:00, 15:00, and 18:00 hora local LT). The IG from the MCD18A1 product has good accuracy with an RMSE of 90 Wm^{-2} [52]. Currently, MCD18A1 spans 8 years: 2004–2011. Meteorological parameters, including, Temperature, relative humidity, and precipitation (rain), were collected using official records from Dirección Meteorológica de Chile (DMC, https://agrometeorologia.cl/).

2.3. Input data validation (satellite and reanalysis)

To validate the database used in this work, the AOD and WV data provided by AERONET (https://aeronet.gsfc.nasa.gov/), last access: October 06, 2023) were used. AERONET uses ground-based Cimel brand sun photometers that measure direct, circum-solar, and sky spectral irradiance every 15 min at different wavelengths (0.340, 0.380, 0.440, 0.500, 0.675, 0.870, 1.020 and 1.640 μm), including the WV absorption band (0.940 μm). Thanks to these measurements, the optical properties of atmospheric constituents can be characterized, as well as the content and other characteristics. AERONET delivers three levels of data quality [53]: Level 1.0 (raw data), Level 1.5 (cloud-filtered and quality-controlled), and Level 2.0 (cloud-filtered and quality-assured). Several studies endorse AERONET as a reference for the validation and adjustment of satellite models and methods delivering AOD and WV products [33,54–56]. For the validation of data, Level 2 observations from 8 AERONET stations distributed in Antofagasta (2), Santiago (4), and Concepción (1) were used (see Table 2).

$$\alpha = -\frac{ln\,(AOD_{440}/AOD_{675})}{ln\,(440/675)} \tag{1}$$

$$AOD_{550} = AOD_{440}(550/440)^{-\alpha} \tag{2}$$

Following Equations (3) and (4), the WV values were calculated, using the value of total precipitable water (pw) and the Ångström index for the wavelength of 440 nm–870nm [58].

$$\alpha = -\frac{ln\,(AOD_{440}/AOD_{870})}{ln\,(870)} \tag{3}$$

$$pw = \frac{pw^{*}AOD_{440}}{AOD_{440} - AOD_{870}{}^{*}\alpha} \tag{4}$$

For ozone evaluation, was used Level-3 Aura/OMI Global Data Products (0.25 deg Lat/Lon grids) available at https://www.earthdata.nasa.gov/. This Level-3 global total column ozone product is derived from OMDOAO3 which is based on the Differential Absorption Spectroscopy (DOAS) fitting technique that uses the OMI visible radiance values between 331.1 nm and 336.1 nm. Studies such as [59], and [60] have reported a strong correlation between Total Ozone Column (TOC) data from the Ozone Monitoring Instrument (OMI) and measurements obtained through observations using the Dobson and Brewer spectrometers.

Table 2
Sites selected for input data validation.

City	Site	Latitude (°S)	Longitude (°W)	Data AERONET
Antofagasta	Paranal_CTA	24.70	70.33	01-01-2015 to 31-12-2019
	PSDA_Chile	24.09	69.93	01-01-2018 to 31-12-2022
Santiago	Santiago	33.49	70.72	01-01-2001 to 31-12-2003
	Santiago_Beauchef_2	33.46	70.66	01-01-2016 to 31- 12-2021
	Campus_USACH	33.45	70.68	01-01-2019 to 31-12-2021
	Yerba_Loca	33.33	70.30	01-01-2020 to 31-12-2022
Concepción	UdecConcepcion-CEFOP	36.84	73.01	01-01-2014 to 31-12-2016

AERONET does not provide observations directly at 550 nm, the Ångström index for the 440 nm-675nm wavelength is used to interpolate the AOD Ångström index at 550 nm (α) [57], and was obtained using Equations (1) and (2).

2.4. Simulation process

The UVSPEC/LibRadtran model is a powerful tool for simulating atmospheric spectral radiative fluxes e. In this simulation modeling strategy, to solve the radiative transfer equation the discrete ordinates method was used [61], and atmospheric profiles for accurate simulations [62]. To facilitate the process, a lookup table (LUT) approach, as described by Ref. [35] was employed. This LUT is a pre-calculated table corresponding to specific input values for atmospheric parameters and sky conditions, which enables the derivation of a parameter K that represents the UVR/IG surface ratio. Equation (5) depicts the relationship proposed for each K estimation, depending on the solar zenith angle, altitude, and atmospheric variables (cloud, AOD, TOC). Tables 2 and 3 provide a list of sources and atmospheric inputs employed here. The atmospheric variables related to the other atmospheric gases are constant according to the type of atmosphere, e.g. tropical, midlatitude, etc. Once these tables are generated, they can be used to quickly find the K value. Subsequently, for each value of the IG product obtained from the MODIS (MCD18A1) every 3 h, UVR was estimated from IG*K multiplication. The time series selected for analysis spanned the years 2004–2011. In addition to the LUTs, certain assumptions are made to

Table 3
The input atmospheric parameters and their ranges used UVSPEC/LibRadtran simulations for clear and cloudy conditions.

Input data	LUTs range
Aerosol optical depth (AOD, nm)	0.1–0.6
Amstrong parameter (AMS, nm)	0.86–2.2
Water vapor (WV, cm)	1.0–6.5
Total ozone column (O_3, DU)	229–369
Integrated Surface albedo	0.11–1.00
Altitude (km)	0.2–6.0
Cosine of solar zenith angle (CSZA)	0.1–1
Cloud optical depth (COD)	10
Effective radius (cloudy) (um)	11.6
Spectral range (nm)	250–4000
Cloud fraction (CF)	0–1
Cloud base (m)	800
Cloud top (m)	2000

simplify the model. For example, clouds' optical and microphysical properties are assumed to be constant, and the same base and top are used. However, these assumptions can be refined by incorporating MODIS cloud properties products (MOD06_L2 and MYD06_L@). We assumed a cloud optical depth and effective radius of 10 and 11.6 μm, respectively. It is recommended that vertical-level variables from ERA5 are not used. Instead, vertically integrated variables such as cloud optical depth, integrated ozone, and WV should be employed. The resulting UVR data are instantaneous values in watts per square meter (Wm^{-2}), which are then integrated into mean and accumulated daily, monthly, and yearly values in kilojoules per square meter (kJm^{-2}) for further analysis. A Typical Meteorological Year (TMY) was calculated from this data.

$$K = f(atmospheric\ variables) \quad (5)$$

2.5. Exploring the viability of solar-powered photo-fenton process for cleaning up wastewater

The solar-derived UVR spectra were integrated over the full UV bandwidth and used to get daily and monthly average values during the mean year (8 years). To get monthly and annual values for Antofagasta, Santiago, and Concepcion, the solar-derived UVR between 9:00, 12:00, 15:00, and 18:00 LT was used. Solar radiation is normally expressed as "Irradiance" (incident power on a surface of a unit area, in Wm^{-2}). Using this data as well as temperature records in combination with the photo-Fenton kinetic model proposed by Ref. [15] the potential viability of the solar-powered photo-Fenton process for cleaning up wastewater in populated Chilean cities can be analyzed. We analyzed the exposure time estimation for water treatment by solar photo-Fenton and the photo reactor volume needed to treat 10 m^3 day^{-1} of water. The simulations were based on paracetamol-contaminated water with a concentration of 100 mg L^{-1} of dissolved organic carbon (DOC) as a representative model wastewater. The designated treatment goal was set at achieving a 75 % removal of DOC. Further information about the model (structure, calibration, and validation) can be found in Ref. [15]. In this way, it was possible to extend the previous analysis by Ref. [17] for the city of Arica to other populated Chilean cities.

3. Results and discussion

In advanced oxidation processes for wastewater treatment, laboratory-scale experiments are very often conducted under constant irradiance conditions inside a solar box. This allows for solar light simulation, although this situation differs from pilot-scale tests under natural solar radiation. According to measurements, solar irradiance instantly varies during the reaction time because of conditions such as cloudiness, rain, particles in the atmosphere, and time of day, which will limit the incidence of UV photons on the photocatalytic system. Therefore, the seasonal variation of some meteorological and atmospheric parameters characteristic of locations under study and their impact on the UVR and performance of solar water treatments will be addressed below.

3.1. Atmospheric conditions in selected locations

Fig. 2a–d shows the seasonal variability of several parameters, including cloud fraction (CF), total ozone column (O_3, DU), Water Vapor (WV, mm), and aerosol (AOD550, nm) for each study site. Other parameters such as Temperature, Accumulated Rain, Relative Humidity, and Global irradiance are shown in Table SI1. The minimum temperature was 9.7 °C (Concepcion) in the winter to a maximum of 21.9 °C (Antofagasta) in the summer. The maximum RH (82.3 %) was observed in Concepcion in July, while the minimum record (44.8 %) was observed during the summer in Santiago. The accumulated precipitation maximum (rainfall) was found in Concepcion with a value of 347.8 mm. The driest period was observed during the summer for Santiago and Antofagasta cities, which did not report any rainfall. Similarly, IG is inversely related to CF. The maximum (725.20 Wm^{-2}) and minimum (246.64 Wm^{-2}) of IG were observed in Antofagasta and Santiago, respectively. Comparatively, the major conditions of CF predominate in Concepcion, with the cloudiest period of the year between April and October. It is important to note that the cloudy conditions increase (CF $\geq$ 0.34) in the summer months as shown in Fig. 2a for Antofagasta city, which is related to the desert climate with a predominant daily cycle of clouds and greater presence during the night and at sunrise [63]. The maximum WV (26.97 mm) shown in Fig. 2c was observed in Antofagasta in July, while the minimum record (44.8 %) was observed during Spring in Concepcion (10.06 mm). The higher AOD550 was found at Antofagasta (AOD550 $\approx$ 0.23 nm) during February (Fig. 2d). This relatively low value is found between values reported by Refs. [28,31,39]. The maximum daily O_3 value (327.10 DU) was observed in Concepcion during September and the minimum value (248.53 DU) was registered during March in Antofagasta Fig. 2b). For all cities, the months between January and May had an $O_3 \leq 276$ DU. The O_3 has a greater impact on the UVR than on global solar radiation [64], which shows higher UVR values may reach the Earth's surface during the summer and autumn in these cities.

3.2. Validation (satellite and reanalysis data)

Previous studies have demonstrated the satisfactory agreement between AERONET and MERRA-2 [33,51,55,56]. In our case, the daily correlation coefficients between AOD and the Antofagasta, Santiago and Concepción measurements range from 0.82 to 0.89. The AOD values from MERRA-2 agree with those from AERONET. These values show an RMSE of less than 0.06 nm for Antofagasta and Concepción and an RMSE of 0.13 nm for Santiago de Chile. In the case of Santiago and Concepción, MERRA-2 underestimates the atmospheric aerosol content, with MBE values of 0.029 and −0.028, respectively. This is due to the high pollution present in the city and the climatic and geographical conditions of the location that favor the occurrence of a stable pollution layer over the city. While high uncertainty values in the AOD do not inherently result in increased error in the estimation of broadband atmospheric radiative transfer or broadband cumulative irradiance [31,51], special care must be taken in how this uncertainty affects the ultraviolet band. Because of this, future campaigns to measure solar irradiance in the ultraviolet range are needed to validate the estimates. Similarly, the WV and O_3 values match those of the AERONET databases. The correlations were found between 0.90 and 0.98 and between 0.96 and 0.99 for WV and O_3, respectively. The RMSE values indicate that the maximum deviation in the O_3 data occurred in Santiago with a value of 7.77 DU, which is relatively low in absolute terms. For the WV values, the maximum deviation occurred in Concepción with a value of 3.40 mm (see Fig. 3).

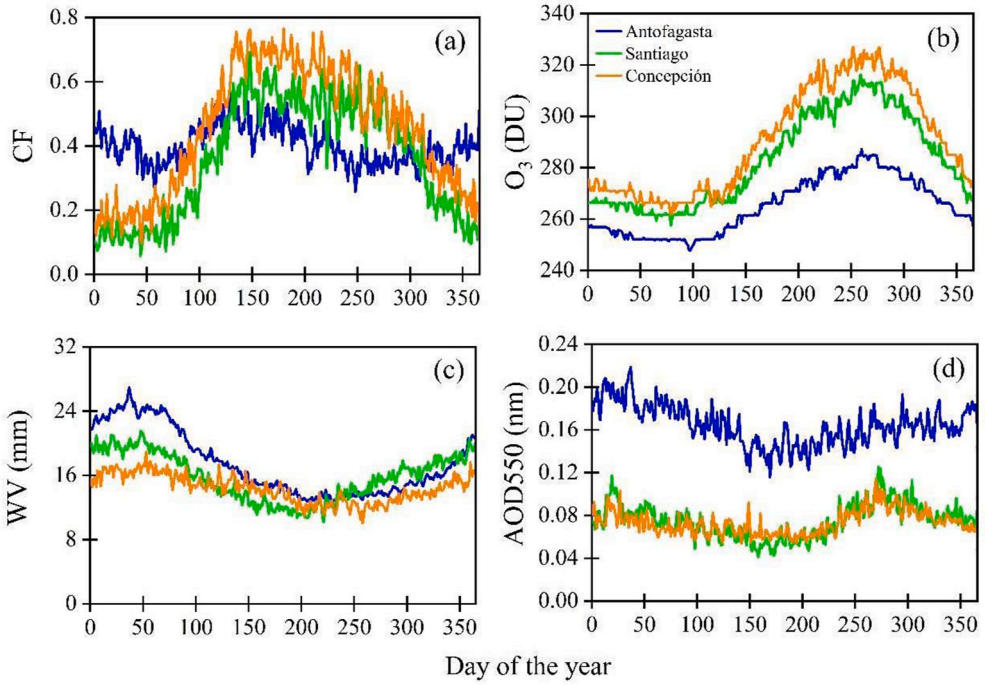

Fig. 2. Daily climatology of (a) CF, (b) O_3, (c) WV, and (d) AOD550 parameters for each study site.

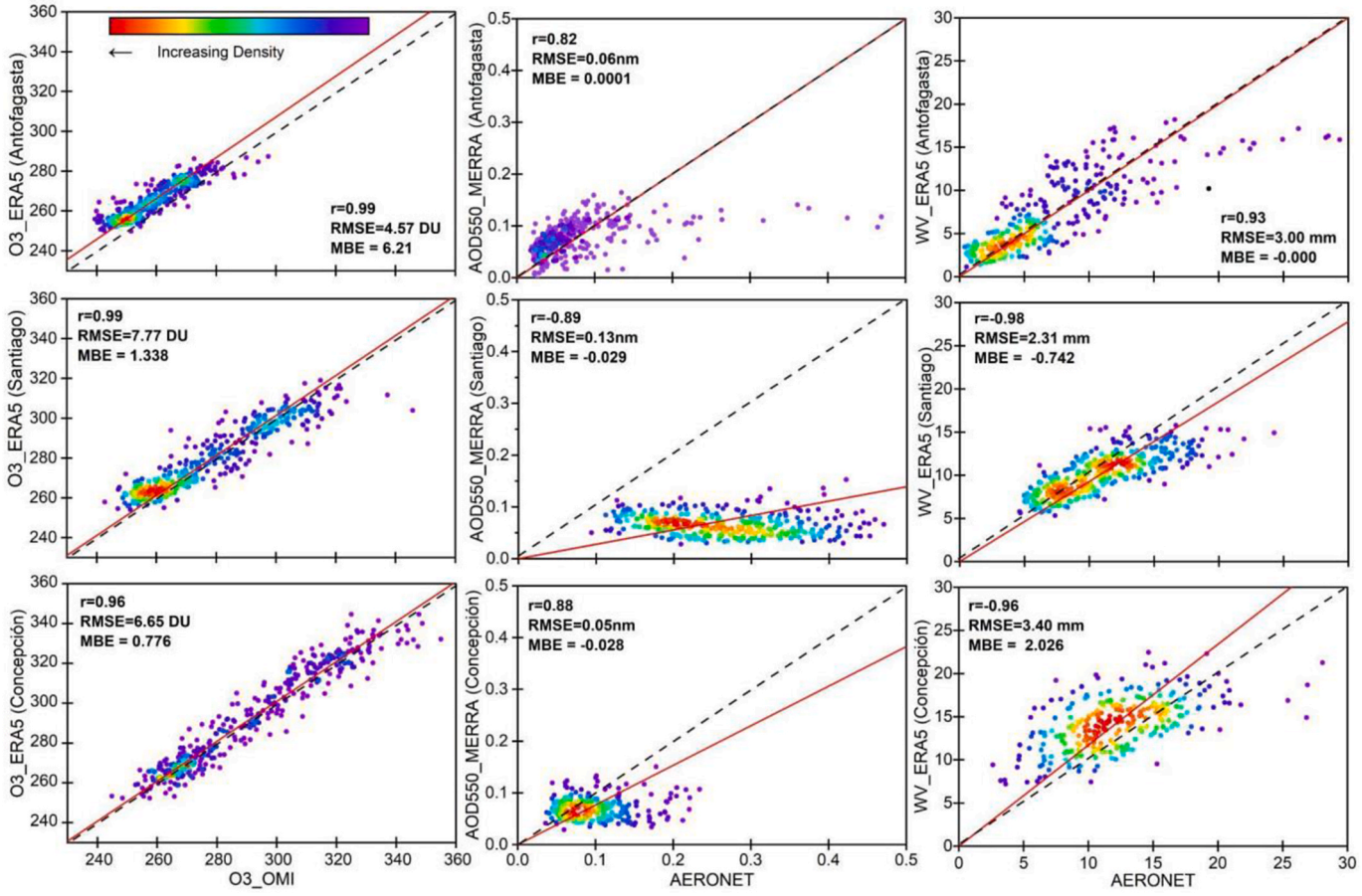

Fig. 3. Daily values of O_3, AOD550, and WV for each study site. The dashed black line is the 1:1 line. Red lines indicate the fitting using the least-squares regression method. Linear regressions are constrained to pass through the origin (0.0).

3.3. Spectral irradiance

Fig. 4 shows solar spectra samples estimated at noon (14:00 LT) from UVSPEC/LibRadtran. Total or global solar radiation measured on a surface is the sum of the beam (direct), reflected, and diffuse radiative components. Direct solar radiation is the solar radiation received from the sunbeam without having been scattered by the atmosphere. The fraction of solar radiation scattered from the sun's beam by the atmosphere is incident on surfaces from the entire sky and is defined as diffuse solar radiation. The main absorption bands correspond to O_3, O_2, and H_2O atmospheric gases. The effect in the spectral distribution is shown in Fig. 4.

3.4. Solar-derived UVR values in irradiance terms

During the summer season, for all the cities studied, the UV irradiance increased until reaching values above 37.67 Wm^{-2}. The monthly UVR minimum values of 15.27 Wm^{-2} and 15.85 Wm^{-2} were found in June for Santiago and Concepcion, respectively. Similar results were found by Ref. [44]. The annual average of solar-derived UVR for each city was 32.81 Wm^{-2} (Antofagasta), 30.07 Wm^{-2} (Santiago), and 28.88 Wm^{-2} (Concepcion). These annual average values are almost double the annual average, for example, in east-southern Spain at Plataforma Solar de Almería (PSA, 37.09°N, −2.36°E, 500 m.a.s.l), or the North of Portugal (41°N, −9.14°W, 104 m.a.s.l) where the first pre-industrial plant for leachates treatment from a sanitary landfill is located (Silva et al., 2016). The annual values of UVR reported for these sites were 18.60 Wm^{-2} [65] and 17.00 Wm^{-2} [66], respectively. Therefore, the solar-derived UVR indicates that for 8 months the values of UVR are systematically larger than 20 Wm^{-2} for Santiago and Concepcion, while in Antofagasta this value is exceeded each month. These are promising results for the potential application of solar water treatments in the cities under study.

3.5. Solar-derived UVR values in irradiation terms

Fig. 5 shows the annual evolution of the daily UVR values for the cities from UVSPEC/LibRadtran. The seasonal variation in the mean values of UVR and IG is mainly caused by astronomical factors (sun declination). However, the variation of UVR and IG of the median, minimum value, and maximum value is probably strongly affected by climate (cloud, RH, precipitation) and environmental conditions (O_3 tropospheric, AOD). The mean daily annual values of IG and UVR were 21.78 ± 4.24 MJm^{-2}, 21.22 ± 2.39 MJm^{-2}, 19.56 ± 2.39 MJm^{-2} and 1406.34 ± 273.70kJm^{-2}, 1300.84 ± 231.00 kJm^{-2}, 1224.14 ± 242.30kJm^{-2}, for Antofagasta, Santiago, Concepcion, respectively. The maximum UVR values occurred during the summer (January) when O_3 and CF are minima (Fig. 2b–a), even in Antofagasta which presents a very high CF during summer (Fig. 2a) ranging from 1714.66 ± 273.51kJm^{-2} until 1791.32 ± 335.98 kJm^{-2}. In contrast, the minimum values of UVR occurred during the winter months when CF is maximum and O_3 increases towards spring maximum (Fig. 2e–d). The average daily values of IG ranged from a minimum of 9.07 MJm^{-2} in Concepcion (June) to a maximum of 31.20 MJm^{-2} in Santiago (January). During winter the air pollution conditions deteriorate in Santiago and Concepcion when the aerosol concentration and other trace gases (nitrogen dioxide and sulfur dioxide) increase [67,68] attenuating the solar radiation beam and contributing to reducing UVR and IG that reaches the surface.

Table 4 shows the most representative statistical indices (mean, median, maximum, minimum, standard deviation (σ), 1st and 3rd quartiles (Q1 and Q3), and 5th and 95th percentiles (P5 and P95) of UVR (in kJm^{-2}) for each month. The median values are mainly slightly higher than the mean; the maximum standard deviation occurs in the October/November months, while the lowest values are in the winter months, so higher stability is observed in these months. The differences between the Max and P95 values are small, for instance, they are smaller than 134.61 kJm^{-2}. However, a large difference between the minimum values and the P5 percentile is more noticeable in the summer. It can be suggested that the absolute minimum values cannot represent the UVR and correspond to outliers. Similar results have been obtained by Ref. [69].

3.6. Exploring the viability of solar-powered photo-fenton process for cleaning up wastewater

Since photochemical reactions depend on the received energy instead of time, UVR data in combination with temperature records can be used to preliminarily evaluate the performance of solar water treatments at different locations or even to calculate the photo reactor surface (process scalability). Fig. 6a illustrates the treatment time needed to achieve the 75 % removal of the dissolved organic carbon (DOC) contained in paracetamol-polluted water by solar photo-Fenton resulting using UVR (TMY) and temperature monthly average values at each location (Antofagasta, Santiago, and Concepción). The lowest treatment times were during the summer months when the highest UVR and temperature values were reached (Fig. 6a). The shortest treatment time for summer operation was observed in Santiago (21 min), followed by Antofagasta (34 min), and Concepción (35 min). The higher local temperature in Santiago, compared to the other two cities, plays a key role in enhancing photo Fenton process performance. However, this order of performance was not the same for winter operations. In winter, which exhibited the highest treatment times in June and July for Concepción, the shortest treatment time was achieved in Antofagasta (62 min). This duration is approximately half the time needed in Concepción, which stands at 120 min, and roughly two-thirds of the time needed in Santiago, 89 min. The consistent solar radiation stability throughout the year in Antofagasta, even during winter, coupled with its mild temperature during the winter period, accounts for the advantages found for Antofagasta. Certainly, the difference between the maximum and minimum treatment times in Antofagasta was notably narrow, amounting to

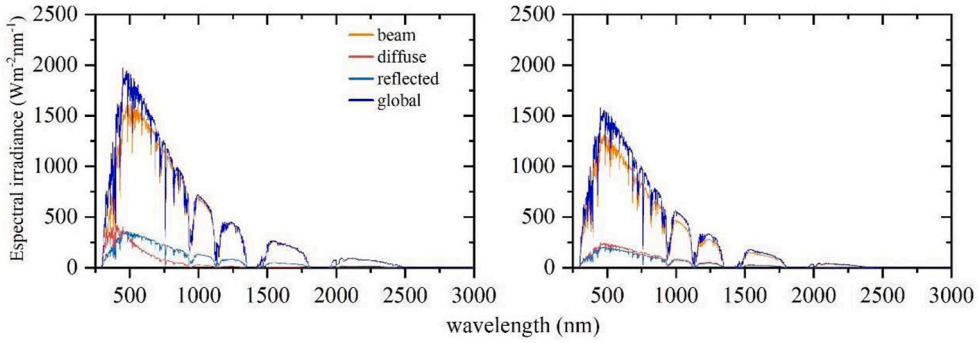

Fig. 4. Solid lines correspond to spectra irradiance derived by the UVSPEC/LibRadtran radiative transfer model for an (a) clear and (b) cloudy day at 14:00 LT.

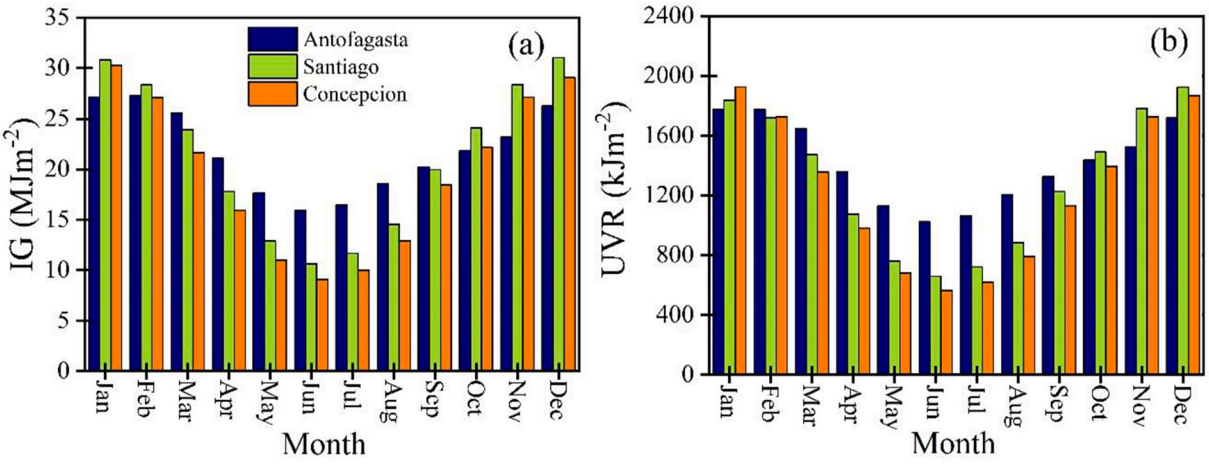

Fig. 5. Seasonal variation of daily values of (a) IG and (b) UVR in Antofagasta, Santiago, and Concepcion.

Table 4
Statistical indices of solar-derived UVR (kJm^{-2}) in Antofagasta, Santiago y Concepcion for the TMY.

Month	Mean	Median	Max	Min	σ	Q1	Q3	P5	P95
Antofagasta									
Jan	1791.32	1822.91	2153.95	647.67	335.98	1722.95	2016.72	1166.44	2142.35
Feb	1744.32	1833.76	2137.04	927.96	298.58	1659.71	1958.32	1256.68	2062.54
Mar	1647.85	1745.46	1948.78	585.33	312.66	1596.47	1843.15	1051.62	1943.46
Apr	1292.83	1414.82	1655.30	648.92	269.38	1209.20	1536.32	808.73	1629.98
May	1123.77	1164.36	1340.86	768.47	134.13	1027.45	1217.19	876.50	1272.62
Jun	1024.92	1074.82	1163.16	773.70	112.78	949.46	1098.37	811.00	1151.06
Jul	1070.54	1096.06	1281.78	591.59	145.56	1026.34	1150.44	829.66	1242.49
Aug	1208.43	1290.15	1520.60	603.98	238.99	1064.10	1348.20	741.73	1485.49
Sep	1322.95	1346.41	1876.50	631.19	331.41	1105.27	1589.62	731.21	1800.69
Oct	1442.36	1516.91	2097.53	784.87	372.16	1252.26	1674.16	819.48	1962.91
Nov	1492.20	1491.30	2149.88	732.02	459.27	1075.27	1872.34	763.04	2140.22
Dec	1714.66	1720.83	2211.72	1180.59	273.51	1573.76	1901.17	1298.89	2116.41
Annual	**1406.35**	**1459.82**	**1794.76**	**739.69**	**273.70**	**1271.85**	**1600.50**	**929.58**	**1745.85**
Santiago									
Jan	1856.56	1888.23	2180.33	785.06	260.32	1722.50	2009.96	1680.93	2128.86
Feb	1708.48	1754.79	1953.51	479.98	276.38	1645.79	1865.74	1440.50	1941.51
Mar	1483.52	1487.08	1783.09	788.78	211.32	1374.68	1632.98	1134.68	1754.02
Apr	1053.02	1107.02	1339.30	481.46	214.69	994.74	1252.55	665.54	1332.43
May	759.83	725.16	1009.93	475.49	148.65	657.03	869.71	545.27	992.16
Jun	655.21	700.83	769.20	456.86	98.55	586.36	725.39	477.02	747.66
Jul	720.60	753.63	900.30	410.36	119.44	687.86	798.03	517.59	884.81
Aug	903.41	918.71	1264.29	397.06	228.12	729.46	1037.73	579.97	1252.08
Sep	1218.93	1351.91	1589.52	413.52	318.27	1030.43	1439.26	637.20	1550.89
Oct	1496.15	1586.19	2016.28	826.69	324.09	1272.32	1742.81	875.57	1883.50
Nov	1809.04	1940.14	2149.14	485.73	383.45	1806.88	2043.46	1081.51	2102.80
Dec	1945.32	1987.09	2179.52	1400.89	188.72	1861.49	2072.02	1565.14	2167.31
Annual	**1300.84**	**1350.06**	**1594.53**	**616.82**	**231.00**	**1197.46**	**1457.47**	**933.41**	**1561.50**
Concepción									
Jan	1939.38	1978.58	2115.14	1610.56	138.28	1847.01	2039.02	1692.23	2111.32
Feb	1719.38	1786.14	2011.54	788.92	293.85	1701.05	1896.19	1075.54	2000.10
Mar	1351.87	1398.86	1682.05	543.94	263.49	1296.51	1513.99	778.69	1664.64
Apr	946.96	975.84	1311.00	640.37	190.70	892.47	1106.58	646.49	1273.39
May	679.94	669.72	879.96	421.15	111.61	600.26	763.12	522.05	840.72
Jun	564.23	567.32	709.54	361.87	81.37	525.64	626.93	436.60	668.91
Jul	616.98	613.58	773.07	447.36	97.11	543.49	702.48	466.46	762.70
Aug	787.48	775.52	1178.82	491.28	180.98	658.93	903.26	523.63	1077.61
Sep	1135.93	1215.12	1614.60	587.82	285.86	970.26	1317.04	631.96	1523.54
Oct	1382.25	1575.03	1957.96	335.47	440.14	1128.91	1694.33	631.40	1887.21
Nov	1713.39	1896.75	2046.87	584.59	390.54	1559.94	1963.59	772.42	2018.84
Dec	1851.94	2056.31	2214.29	432.34	433.69	1767.04	2109.19	966.60	2162.70
Annual	**1224.14**	**1292.40**	**1541.24**	**603.81**	**242.30**	**1124.29**	**1386.31**	**762.01**	**1499.31**

only 28 min (34–62 min). In contrast, this difference expands considerably in Santiago, where it reached 68 min (21–89 min), and even more so in Concepción, where it reached 85 min (35–120 min). Indeed, Concepción always presented the highest treatment time independently of the selected month. These results show that the treatment of pollutants by solar photo-Fenton is possible in assumable times, with the UVR recorded in the three cities of Chile.

The treatment time required to achieve the decontamination goal is a crucial factor in evaluating process performance. However, it is essential not to overlook the availability of sunlight at each specific location. By dividing the annual or monthly sun hours available at each location by the corresponding treatment time, the number of batches that can be

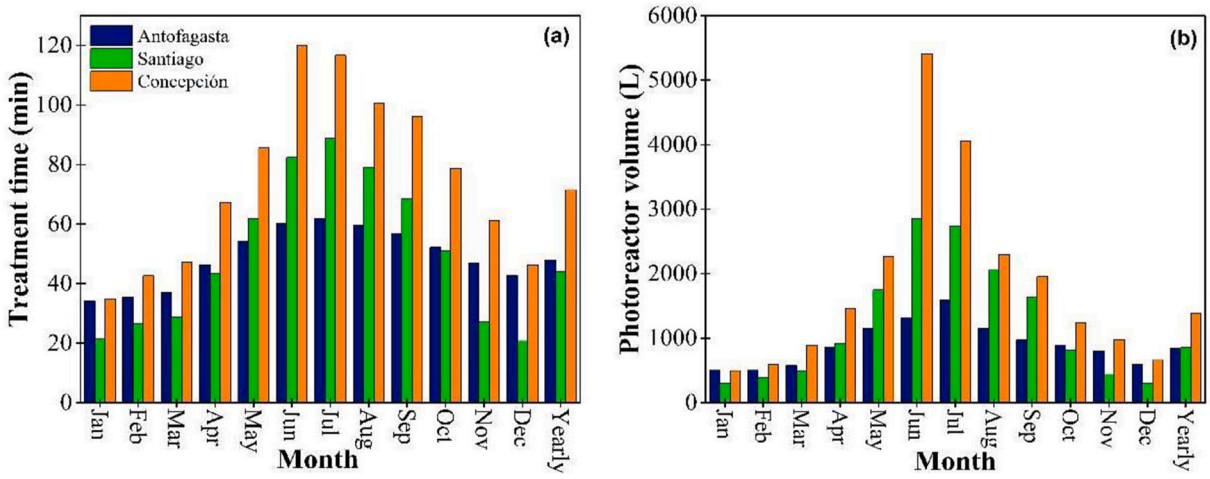

Fig. 6. (a) Estimation of the treatment time needed to reach 75 % degradation of paracetamol polluted water, (b) Estimation of the photo reactor volume needed to treat 10 m^3 day^{-1} of polluted water based on UVR and temperature monthly and yearly average values got from the TMY.

conducted per year or month can be determined. This approach allows an estimate of the required photo reactor volume for an application, as outlined by Ref. [15], by dividing the treatment volume aim in a certain period by the number of batches that can be conducted during the same period. It is important to note that the size of the photo reactor is directly linked to the investment cost and, consequently; it is a critical factor in assessing the feasibility of the overall process. Fig. 6b shows an estimation of the photo reactor volume needed to treat 10 m^3 day^{-1} of paracetamol-polluted water. This estimation is derived from the monthly and yearly average values of UVR, and temperature extracted from the TMY dataset. The trends in Fig. 6a and b are quite similar, i.e. Santiago still presents the lowest photo reactor volume during summer (297 L) and Antofagasta during winter (1589 L), with Concepción presenting the highest photoreactor volume throughout the year (498–5412 L). The differences between cities became more pronounced in winter and decreased during summer. The primary contributing factors to this phenomenon are, on one hand, the significantly greater abundance of sunlight in Antofagasta during the winter months concerning Santiago and Concepción, and the previously discussed daily cloud cycle during the summer months in Antofagasta. This cloud cycle is associated with the desert climate and results in a reduction of available solar hours for treatment. Determining the most suitable month for process scalability demands thorough research. However, UVR datasets are of utmost importance since they offer in-depth insights into process performance and help to make critical decisions, such as selecting the ideal location of a pilot plant or industry.

Hence, it has been established that the availability of solar radiation data is essential for solar water treatments. However, it is equally crucial to underscore the critical significance of the solar spectrum in simulating solar water treatments [70]. Presently, a multitude of studies are focusing on the development of novel photocatalysts with a wide range of optical properties [8,71–73]. Given that each photocatalyst possesses a unique absorption spectrum, it becomes imperative to grasp the variations in the solar spectrum across various locations. Solely depending on a single UVR value may lead to substantial disparities in the prediction of Solar photo-Fenton process performance. Furthermore, environmental factors like water turbidity, color, and dissolved substances can exert an influence on the transmission and absorption of UVR in column water. Higher turbidity or the presence of organic matter can diminish the amount of available UVR, consequently affecting the efficiency of the Solar photo-Fenton process. Moreover, radiation alone does not contribute to the best performance of solar technologies, since other operating parameters, e.g., catalyst concentration, pollutant concentration, pH, temperature, etc., must be also considered. Additionally, it is worth noting that certain authors mention UVR without providing specific details, such as the wavelength range encompassed by the measurement, the duration of the measurement, or the radiometric equipment utilized. This lack of precision can potentially result in significant errors. The significance of this study is underscored by its preliminary assessment of the spectral UVR effects on the performance of outdoor Solar photo-Fenton experiments for the Chilean region.

4. Limitations

Despite the benefits of the approach presented in this study, there are some limitations and challenges that should be addressed. To improve the K ratio, it is necessary to consider site characteristics, e.g., land use or albedo [74]. It is important to stress that, since these are solar-derived UVR values from the UVSPEC/LibRadtran model, having ground-based measurements for validation is a current limitation. Therefore, validation of the performance of the LibRadtran model will be carried out through further investigation using UVR ground-based measurements. However, the present contribution can be considered the basis for future studies related to spatiotemporal distributions of solar UVR in Chile.

5. Conclusions

The analysis showed the possibilities of exploiting the potential of Solar photo-Fenton in populated Chilean cities to provide tools for the integration of solar energy in water treatment technologies.

1. The UVSPEC/LibRadtran RTM was applied in three Chilean cities with different climatic zones, to obtain solar-derivate UVR values. The input data for the model include altitude, latitude, CF, O_3, WV, and AOD parameters.
2. Based on the analysis performed, it can be concluded that solar photocatalysis is indeed feasible in competitive treatment times for most of the cases reported in this study, with the UVR values reached between latitudes (−24°S until −37°S). Antofagasta, owing to its solar radiation stability, high number of solar hours, and mild climate, stands out as a location offering exceptional conditions for the implementation of solar water treatment applications.
3. This research motivates further studies on spectral radiation and emerging advanced oxidation technologies and the development of prospects for water and wastewater treatment.

Data availability

Solar-derived UVR data used in this study are available on request to Lisdelys González-Rodríguez.

CRediT authorship contribution statement

Lisdelys González-Rodríguez: Writing – review & editing, Writing – original draft, Visualization, Validation, Software, Resources, Project administration, Methodology, Investigation, Funding acquisition, Formal analysis, Data curation, Conceptualization. **Alex Cabrera:** Writing – review & editing, Writing – original draft, Visualization, Validation, Software, Methodology, Investigation. **Jorge Rosas:** Writing – review & editing, Writing – original draft, Software, Methodology, Investigation, Formal analysis, Data curation. **Matías Volke:** Writing – review & editing, Visualization, Validation, Software, Methodology, Formal analysis, Data curation. **Aitor Marzo:** Writing – review & editing, Writing – original draft, Visualization, Validation, Software, Resources, Project administration, Methodology, Investigation, Funding acquisition, Formal analysis.

Declaration of competing interest

The authors declare that they have no known competing financial interests or personal relationships that could have appeared to influence the work reported in this paper.

Acknowledgments

Lisdelys González R. thanks the competitive Fund for Regular Research Projects 2023 granted by UDLA. Alejandro Cabrera Reina wants to thank ANID/FONDECYT/1230704 and ANID/FONDAP/1523A0006. The authors want to acknowledge the project HELIOSUN, with reference PID2021-126805OB-I00, financed by Ministerio de Ciencia e Innovación, and co-financed by the European Regional Development Fund. A. Marzo thanks for the Ramon y Cajal contract (RYC2021-031958-I), funded by Spanish Ministerio de Ciencia e Innovación MCIN/AEI/10.13039/501100011033 and by "European Union NextGenerationEU/PRTR". The authors thank MODIS, OMI, ERA, and MERRA for making the satellite and reanalysis data available for public use. Funding for open access charge: Universidad de Granada/CBUA.

Appendix A. Supplementary data

Supplementary data to this article can be found online at https://doi.org/10.1016/j.renene.2024.121078.

References

[1] L. Rodríguez-López, A. Lami, M. El Ouahabi, N. Fagel, D. Álvarez, L. González-Rodríguez, S. Schmidt, R. Urrutia, Fossil pigments and environmental conditions in the oligotrophic Laja Lake in the Chilean Andes, Anthropocene 37 (2022), https://doi.org/10.1016/j.ancene.2022.100321.

[2] L. González-Rodríguez, J. Jiménez, L. Rodríguez-López, A.P. de Oliveira, A. C. Baeza, D. Contreras, L. Pérez-Hernández, Ultraviolet erythemal radiation in Central Chile: direct and indirect implication for public health, Air Qual Atmos Health 14 (2021) 1533–1548, https://doi.org/10.1007/s11869-021-01037-3.

[3] J. Blanco Malato, A. Vidal, C. Richter, Photocatalysis with solar energy at a pilot-plant scale: an overview, Appl. Catal., B 37 (2002) 1–15, https://doi.org/10.1016/S0926-3373(01)00315-0.

[4] S. Malato, P. Fernández-Ibáñez, M.I. Maldonado, J. Blanco, W. Gernjak, Decontamination and disinfection of water by solar photocatalysis: recent overview and trends, Catal. Today 147 (2009) 1–59, https://doi.org/10.1016/j.cattod.2009.06.018.

[5] Á. García-gil, R. Valverde, R.A. García-muñoz, K.G. Mcguigan, J. Marugán, Solar water disinfection in high-volume containers : are naturally occurring substances attenuating factors of radiation, Chem. Eng. J. 399 (2020) 125852, https://doi.org/10.1016/j.cej.2020.125852.

[6] J.I. Ajona, A. Vidal, The use of CPC collectors for detoxification of contaminated water: design, construction and preliminary results, Sol. Energy 68 (2000) 109–120, https://doi.org/10.1016/S0038-092X(99)00047-X.

[7] S. Malato, M.I. Maldonado, P. Fernández-ibáñez, I. Oller, I. Polo, R. Sánchez-moreno, Decontamination and disinfection of water by solar photocatalysis : The pilot plants of the Plataforma Solar de Almeria, Mater. Sci. Semicond. Process. 42 (2016) 15–23, https://doi.org/10.1016/j.mssp.2015.07.017.

[8] G. Lofrano, G. Libralato, A. Casaburi, A. Siciliano, P. Iannece, M. Guida, L. Pucci, E. F. Dentice, M. Carotenuto, Municipal wastewater spiramycin removal by conventional treatments and heterogeneous photocatalysis, Sci. Total Environ. 624 (2018) 461–469, https://doi.org/10.1016/j.scitotenv.2017.12.145.

[9] A. Cabrera-Reina, S. Miralles-cuevas, G. Rivas, J.A.S. Pérez, Comparison of different detoxi fication pilot plants for the treatment of industrial wastewater by solar photo-Fenton: are raceway pond reactors a feasible option, Sci. Total Environ. 648 (2019) 601–608, https://doi.org/10.1016/j.scitotenv.2018.08.143.

[10] A. Cabrera-Reina, S. Miralles-Cuevas, P. Soriano-Molina, J.A. Sánchez-Pérez, A critical evaluation of the use of accumulated energy as a parameter for the scale-up of solar photoreactors during the treatment of simulated industrial wastewater by solar photo-Fenton, J. Chem. Technol. Biotechnol. 96 (2021) 1593–1602, https://doi.org/10.1002/jctb.6678.

[11] S. Malato, J. Blanco, C. Richter, M.I. Maldonado, Optimization of pre-industrial solar photocatalytic mineralization of commercial pesticides: application to pesticide container recycling, Appl. Catal., B 25 (2000) 31–38, https://doi.org/10.1016/S0926-3373(99)00114-9.

[12] Pereira, J.P. Vilar, M.T. Borges, O. Gonza, S. Esplugas, R.A.R. Boaventura, Photocatalytic degradation of oxytetracycline using TiO2 under natural and simulated solar radiation, Sol. Energy 85 (2011) 2732–2740, https://doi.org/10.1016/j.solener.2011.08.012.

[13] I. De la Obra Jiménez, J.L.C. López, G.R. Ibáñez, B.E. García, J.A.S. Pérez, Kinetic assessment of antibiotic resistant bacteria inactivation by solar photo-Fenton in batch and continuous flow mode for wastewater reuse, Water Res. 159 (2019) 184–191, https://doi.org/10.1016/j.watres.2019.04.059.

[14] E.G. Mbonimpa, E.R. Blatchley, B. Applegate, W.F. Harper, Ultraviolet A and B wavelength-dependent inactivation of viruses and bacteria in the water, J. Water Health (2018) 796–806, https://doi.org/10.2166/wh.2018.071.

[15] A. Cabrera Reina, J.L. Casas López, M.I. Maldonado Rubio, L. Santos-Juanes Jordá, J.L. García Sánchez, J.A. Sánchez Pérez, Effects of environmental variables on the photo-Fenton plant design, Chem. Eng. J. 237 (2014) 469–477, https://doi.org/10.1016/j.cej.2013.10.046.

[16] A. Zapata, I. Oller, L. Rizzo, S. Hilgert, M.I. Maldonado, J.A. Sánchez-Pérez, S. Malato, Evaluation of operating parameters involved in solar photo-Fenton treatment of wastewater: interdependence of initial pollutant concentration, temperature and iron concentration, Appl. Catal., B 97 (2010) 292–298, https://doi.org/10.1016/j.apcatb.2010.04.020.

[17] A. Cabrera Reina, S. Miralles-Cuevas, L. Cornejo, L. Pomares, J. Polo, I. Oller, S. Malato, The influence of location on solar photo-Fenton: process performance, photoreactor scaling-up and treatment cost, Renew. Energy 145 (2020) 1890–1900, https://doi.org/10.1016/j.renene.2019.07.113.

[18] A. Cabrera Reina, L. Santos-Juanes, J.L. García Sánchez, J.L. Casas López, M. I. Maldonado Rubio, G. Li Puma, J.A. Sánchez Pérez, Modelling the photo-Fenton oxidation of the pharmaceutical paracetamol in water including the effect of photon absorption (VRPA), Appl. Catal., B 166–167 (2015) 295–301, https://doi.org/10.1016/j.apcatb.2014.11.023.

[19] S. Samoili, G. Farinelli, J.Á. Moreno-SanSegundo, K.G. McGuigan, J. Marugán, C. Pulgarín, S. Giannakis, Predicting the bactericidal efficacy of solar disinfection (SODIS): from kinetic modeling of in vitro tests towards the in silico forecast of E. coli inactivation, Chem. Eng. J. 427 (2021), https://doi.org/10.1016/j.cej.2021.130866.

[20] Y. Xiangwei, M. Graells, S. Miralles-Cuevas, A. Cabrera-Reina, M. Pérez-Moya, An improved hybrid strategy for online dosage of hydrogen peroxide in photo-Fenton processes, J. Environ. Chem. Eng. 9 (2021), https://doi.org/10.1016/j.jece.2021.105235.

[21] P. Soriano-Molina, J.L. García Sánchez, S. Malato, P. Plaza-Bolaños, A. Agüera, J. A. Sánchez Pérez, On the design and operation of solar photo-Fenton open reactors for the removal of contaminants of emerging concern from WWTP effluents at neutral pH, Appl. Catal., B 256 (2019) 117801, https://doi.org/10.1016/j.apcatb.2019.117801.

[22] G. Palma, A. Śnchez, Y. Olave, F. Encina, R. Palma, R. Barra, Pesticide levels in surface waters in an agricultural-forestry basin in Southern Chile, Chemosphere 57 (2004) 763–770, https://doi.org/10.1016/j.chemosphere.2004.08.047.

[23] K. Cooman, P. Debels, M. Gajardo, R. Urrutia, R. Barra, Use of Daphnia spp. for the ecotoxicological assessment of water quality in an agricultural watershed in South-Central Chile, Arch. Environ. Contam. Toxicol. 48 (2005) 191–200, https://doi.org/10.1007/s00244-004-0218-6.

[24] P. Pino, V. Iglesias, R. Garreaud, S. Cortés, M. Canals, W. Folch, S. Burgos, K. Levy, L.P. Naeher, K. Steenland, Chile confronts its environmental health future after 25 years of accelerated growth, Ann Glob Health 81 (2015) 354–367, https://doi.org/10.1016/j.aogh.2015.06.008.

[25] O. Rozas, C. Vidal, C. Baeza, W.F. Jardim, A. Rossner, H.D. Mansilla, Organic micropollutants (OMPs) in natural waters: oxidation by UV/H2O2 treatment and toxicity assessment, Water Res. 98 (2016) 109–118, https://doi.org/10.1016/j.watres.2016.03.069.

[26] M.J. Climent, E. Herrero-Hernández, M.J. Sánchez-Martín, M.S. Rodríguez-Cruz, P. Pedreros, R. Urrutia, Residues of pesticides and some metabolites in dissolved and particulate phase in surface stream water of Cachapoal River basin, central Chile, Environ. Pollut. 251 (2019) 90–101, https://doi.org/10.1016/j.envpol.2019.04.117.

[27] L. Gonzalez Rodríguez, P. A, L. de Oliveira, J. Rodriguez Lopez, D. Rosas, A.C. Baeza Contreras, A study of UVER in Santiago , Chile based on long-term in situ measurements (five years) and empirical modelling, Energies 14 (2021) 21, https://doi.org/10.3390/en14020368.

[28] R.R. Cordero, A. Damiani, G. Seckmeyer, J. Jorquera, M. Caballero, P. Rowe, J. Ferrer, R. Mubarak, J. Carrasco, R. Rondanelli, M. Matus, D. Laroze, The solar

spectrum in the atacama desert, Sci. Rep. 6 (2016) 1–15, https://doi.org/10.1038/srep22457.
[29] L. Vuilleumier, T. Harris, A. Nenes, C. Backes, D. Vernez, Developing a UV climatology for public health purposes using satellite data, Environ. Int. 146 (2021) 106177, https://doi.org/10.1016/j.envint.2020.106177.
[30] A. Damiani, R.R. Cordero, S. Cabrera, M. Laurenza, C. Rafanelli, Cloud cover and UV index estimates in Chile from satellite-derived and ground-based data, Atmos. Res. 138 (2014) 139–151, https://doi.org/10.1016/j.atmosres.2013.11.006.
[31] A. Marzo, A. Salmon, J. Polo, J. Ballestrín, G. Soto, G. Quiñones, J. Alonso-Montesinos, E. Carra, M. Ibarra, J. Cardemil, E. Fuentealba, R. Escobar, Solar extinction map in Chile for applications in solar power tower plants, comparison with other places from sunbelt and impact on LCOE, Renew. Energy 170 (2021) 197–211, https://doi.org/10.1016/j.renene.2021.01.126.
[32] D. Wang, S. Liang, Y. Zhang, X. Gao, M.G.L. Brown, A new set of MODIS land products (MCD18): downward shortwave radiation and photosynthetically active radiation, Rem. Sens. 12 (2020) 15.
[33] C.A. Gueymard, D. Yang, Worldwide validation of CAMS and MERRA-2 reanalysis aerosol optical depth products using 15 years of AERONET observations, Atmos. Environ. 225 (2020) 117216, https://doi.org/10.1016/j.atmosenv.2019.117216.
[34] W. Qin, L. Wang, J. Wei, B. Hu, X. Liang, A novel efficient broadband model to derive daily surface solar Ultraviolet radiation (0.280–0.400 μm), Sci. Total Environ. 735 (2020), https://doi.org/10.1016/j.scitotenv.2020.139513.
[35] J. Verdebout, A satellite-derived UV radiation climatology over europe to support impact studies, in: Arctic-Alpine Ecosystems and People in a Changing Environment, 2004, pp. 357–363.
[36] B. Arbara, a G. Ilchrest, P.E.H.D. Ller, A. Lan, C.G. Eller, M. Ina, Y. Aar, Aurora advanced ultraviolet radiation and ozone retrieval for applications. Description of the Uv Radiation Model with Quality Assessment of the Fields Required by the Demonstrational Applications, 2018.
[37] J. Bak, X. Liu, R. Spurr, K. Yang, C.R. Nowlan, C. Chan Miller, G. Gonzalez Abad, K. Chance, Radiative transfer acceleration based on the principal component analysis and lookup table of corrections: optimization and application to UV ozone profile retrievals, Atmos. Meas. Tech. 14 (2021) 2659–2672, https://doi.org/10.5194/amt-14-2659-2021.
[38] B. Mayer, A. Kylling, Technical note: the libRadtran software package for radiative transfer calculations - description and examples of use, Atmos. Chem. Phys. 5 (2005) 1855–1877, https://doi.org/10.5194/acp-5-1855-2005.
[39] A. Marzo, P. Ferrada, F. Beiza, P. Besson, J. Alonso-Montesinos, J. Ballestrín, R. Román, C. Portillo, R. Escobar, E. Fuentealba, Standard or local solar spectrum? Implications for solar technologies studies in the Atacama desert, Renew. Energy 127 (2018) 871–882, https://doi.org/10.1016/j.renene.2018.05.039.
[40] Chilean Ministry of Energy, Modelo De Transferencia Radiativa Para El Espectro Solar, Herramienta de análisis de la caracterización espectral de la radiación solar del desierto de Atacama para mejorar la competitividad de la industria solar en Chile", Chile, 2020.
[41] M. Antón, L. Alados-Arboledas, J.L. Guerrero-Rascado, M.J. Costa, J. C Chiu, F. J. Olmo, Experimental and modeled UV erythemal irradiance under overcast conditions: the role of cloud optical depth, Atmos. Chem. Phys. 12 (2012) 11723–11732, https://doi.org/10.5194/acp-12-11723-2012.
[42] R. Roman, Reconstrucción y análisis de la radiación ultravioleta eritemática en la Península Ibérica desde 1950. http://www.tdx.cat/bitstream/handle/10803/6493/03IMaj03de11.pdf?sequence=3, 2014.
[43] C. Lovengreen, H.F. Alvarez, José Luis, y M. Aritio, Erythemal Ultraviolet Radiation in Valdivia. A comparison among satellite data, a radiative transfer model and ground-based observations, Rev. Med. Chile 130 (2002).
[44] R.R. Cordero, A. Damiani, J. Jorquera, E. Sepúlveda, M. Caballero, S. Fernandez, S. Feron, P.J. Llanillo, J. Carrasco, D. Laroze, F. Labbe, Ultraviolet radiation in the atacama desert, Antonie van Leeuwenhoek, International Journal of General and Molecular Microbiology 111 (2018) 1301–1313, https://doi.org/10.1007/s10482-018-1075-z.
[45] DGA, Atlas del Agua, Atlas Del Agua Chile 1, 2016, 24, https://dga.mop.gob.cl/.
[46] González-Rodríguez, L. Pérez, A. Fissore, L. Rodríguez-López, J. Jimenez, Tilt and orientation of a flat solar collector to capture optimal solar irradiation in Chilean latitudes, in: In: Springer (Ed.), Proceedings of the 2nd International Conference on BioGeoSciences, 2017, pp. 215–228.
[47] L. Wald, Elements on the Computation of UV Maps in the Eurosun Database, 2012.
[48] H. Hersbach, B. Bell, P. Berrisford, A. Horányi, J.M. Sabater, J. Nicolas, R. Radu, D. Schepers, A. Simmons, C. Soci, D. Dee, Global Reanalysis: Goodbye ERA-Interim, Hello ERA5, ECMWF Newsletter, 2019, pp. 17–24, https://doi.org/10.21957/vf291hehd7.
[49] Agustín Laguarda, Gonzalo Abal, Impacto de la incertidumbre de las variables atmosféricas de la base merra-2 en el modelado de la irradiancia solar en cielo despejado, ASADES 24 (2020) 1–10.
[50] A. Marzo, A. Salmon, J. Polo, J. Ballestrín, G. Soto, G. Quiñones, J. Alonso-Montesinos, E. Carra, M. Ibarra, J. Cardemil, E. Fuentealba, R. Escobar, Solar extinction map in Chile for applications in solar power tower plants, comparison with other places from sunbelt and impact on LCOE, Renew. Energy 170 (2021) 197–211, https://doi.org/10.1016/j.renene.2021.01.126.
[51] A. Salmon, G. Quiñones, G. Soto, J. Polo, C. Gueymard, M. Ibarra, J. Cardemil, R. Escobar, A. Marzo, Advances in aerosol optical depth evaluation from broadband direct normal irradiance measurements, Sol. Energy 221 (2021) 206–217, https://doi.org/10.1016/j.solener.2021.04.039.
[52] S. Liang, D. Wang, Moderate Resolution Imaging Spectroradiometer (MODIS) Downward Shortwave Radiation (MCD18A1) and Photosynthetically Active Radiation (MCD18A2) Algorithm Theoretical Basis Document Collection 6 Change History Log, 2017.
[53] D.M. Giles, A. Sinyuk, M.G. Sorokin, J.S. Schafer, A. Smirnov, I. Slutsker, T.F. Eck, B.N. Holben, J.R. Lewis, J.R. Campbell, E.J. Welton, S. V Korkin, A.I. Lyapustin, Advancements in the Aerosol Robotic Network (AERONET) Version 3 Database – Automated Near-Real-Time Quality Control Algorithm with Improved Cloud Screening for Sun Photometer Aerosol Optical Depth (AOD) Measurements, 2019, pp. 169–209.
[54] J.M. Bright, C.A. Gueymard, Climate-specific and global validation of MODIS Aqua and Terra aerosol optical depth at 452 AERONET stations, Sol. Energy 183 (2019) 594–605, https://doi.org/10.1016/j.solener.2019.03.043.
[55] M. Aldabash, F.B. Balcik, P. Glantz, Validation of MODIS C6.1 and MERRA-2 AOD using AERONET observations: a comparative study over Turkey, Atmosphere 11 (2020), https://doi.org/10.3390/ATMOS11090905.
[56] R.C. Ssenyunzi, B. Oruru, F.M. D'ujanga, E. Realini, S. Barindelli, G. Tagliaferro, A. von Engeln, N. van de Giesen, Performance of ERA5 data in retrieving precipitable water vapour over east african tropical region, Adv. Space Res. 65 (2020) 1877–1893, https://doi.org/10.1016/j.asr.2020.02.003.
[57] W. Qin, H. Fang, L. Wang, J. Wei, M. Zhang, X. Su, M. Bilal, X. Liang, MODIS high-resolution MAIAC aerosol product: global validation and analysis, Atmos. Environ. 264 (2021), https://doi.org/10.1016/j.atmosenv.2021.118684.
[58] V.S. Martins, A. Lyapustin, Y. Wang, D.M. Giles, A. Smirnov, I. Slutsker, S. Korkin, Global validation of columnar water vapor derived from EOS MODIS-MAIAC algorithm against the ground-based AERONET observations, Atmos. Res. 225 (2019) 181–192, https://doi.org/10.1016/j.atmosres.2019.04.005.
[59] J.L. Gómez-Amo, V. Estellés, A. di Sarra, R. Pedrós, D. Sferlazzo, M.P. Utrillas, J. A. Martinez-Lozano, A comparison of Microtops II and satellite ozone measurements in the period 2001-2011, J. Atmos. Sol. Terr. Phys. 94 (2013) 5–12, https://doi.org/10.1016/j.jastp.2012.12.012.
[60] A. Sharma, N. Ojha, A. Pozzer, K.A. Mar, G. Beig, J. Lelieveld, S.S. Gunthe, WRF-Chem simulated surface ozone over south Asia during the pre-monsoon: effects of emission inventories and chemical mechanisms, Atmos. Chem. Phys. 17 (2017) 14393–14413, https://doi.org/10.5194/acp-17-14393-2017.
[61] K. Stamnes, S.-C. Tsay, W. Wiscombe, K. Jayaweera, Numerically stable algorithm for discrete-ordinate-method radiative transfer in multiple scattering and emitting layered media, Appl. Opt. 27 (1988) 2502, https://doi.org/10.1364/ao.27.002502.
[62] G.P. Anderson, S.A. Clough, F.X. Kneizys, J.H. Chetwynd, P. E, Shettle, AFGL Atmospheric Constituent Profiles (0.120 Km), 1986.
[63] P. Osses, R. Escobar, C. del Rio, R. Garcia, C. Vargas, El clima desértico costero con nublados abundantes del desierto de atacama y su relación con los recursos naturales energía solar y agua de niebla. Caso de estudio alto patache (20,5°S), región de tarapacá, Chile, Rev. Geogr. Norte Gd. 48 (2017) 33–48, https://doi.org/10.4067/S0718-34022017000300033.
[64] A.R. Esteve, J.A. Martinez-Lozano, M.J. Marín, V. Estellés, F. Tena, M.P. Utrillas, The influence of ozone and aerosols on the experimental values of UV erythemal radiation at ground level in Valencia, Int. J. Climatol. 2182 (2009) 2171–2182, https://doi.org/10.1002/joc.
[65] S. Malato, J. Blanco, A.R. Fernández-Alba, A. Agüera, Solar photocatalytic mineralization of commercial pesticides: Oxamyl, Chemosphere 40 (2003) 403–409, https://doi.org/10.1016/s0045-6535(99)00267-2.
[66] T.F.C.V. Silva, A. Fonseca, I. Saraiva, R.A.R. Boaventura, V.J.P. Vilar, Scale-up and cost analysis of a photo-Fenton system for sanitary landfill leachate treatment, Chem. Eng. J. 283 (2016) 76–88, https://doi.org/10.1016/j.cej.2015.07.063.
[67] L. Gallardo, G. Olivares, J. Langner, B. Aarhus, Coastal lows and sulfur air pollution in Central Chile, Atmos. Environ. 36 (2002) 3829–3841, https://doi.org/10.1016/S1352-2310(02)00285-6.
[68] C. Mardones, A. Saavedra, J. Jiménez, Cuantificación económica de los beneficios en salud asociados a la reducción de la contaminación por MP10 en Concepción Metropolitano, Chile, Rev. Med. Chile 143 (2015) 475–483, https://doi.org/10.4067/s0034-98872015000400009.
[69] S.A. Kalogirou, S. Pashiardis, A. Pashiardi, Statistical analysis and inter-comparison of erythemal solar radiation for Athalassa and Larnaca, Cyprus, Renew. Energy 111 (2017) 580–597, https://doi.org/10.1016/j.renene.2017.04.043.
[70] C. Casado, Á. García-Gil, R. van Grieken, J. Marugán, Critical role of the light spectrum on the simulation of solar photocatalytic reactors, Appl. Catal., B 252 (2019) 1–9, https://doi.org/10.1016/j.apcatb.2019.04.004.
[71] D. Contreras, V. Melin, G. Pérez-González, A. Henríquez, L. González, Advances and Challenges in BiOX (X: Cl, Br, I)-Based Materials for Harvesting Sunlight, 2020, https://doi.org/10.1007/978-3-030-15608-4_10.
[72] V. Etacheri, C. Di, J. Schneider, D. Bahnemann, S.C. Pillai, Visible-light activation of TiO2 photocatalysts: advances in theory and experiments, J. Photochem. Photobiol. C Photochem. Rev. 25 (2015) 1–29.
[73] Simranjeet Singh, V. Kumar, Daljeet Singh Dhanja, Shivika Datta, Sukhmanpreet Kaur, Romina Romero, Joginder Singh, Degradation of pesticides in wastewater using heterogeneous photocatalysis, in: Maulin P. Shah (Ed.), Advanced Oxidation Processes for Effluent Treatment Plants, Elsevier, 2021, pp. 161–175.
[74] Cordero, Damiani, Ferrer Alessandro, J. Jorquera Jorge, M. Tobar, F. Labbe, J. Carrasco, D. Laroze, UV irradiance and albedo at union glacier camp (Antarctica): a case study, PLoS One 9 (2014), https://doi.org/10.1371/journal.pone.0090705.